Hyperspectral imaging for detection of cholesterol in human skin

Matija Milanic[*a], Asgeir Bjorgan[a], Marcus Larsson[b], Paolo Marraccini[c],Tomas Strömberg[b], Lise Lyngsnes Randeberg[a]

[a]Department of Electronics and Telecommunications, Norwegian University of Science and Technology, Trondheim, Norway
[b]Department of Biomedical Engineering. Linköping University, Linköping, Sweden.
[c]CNR - Istituto di fisiologia clinica, Pisa, Italy

ABSTRACT

Hypercholesterolemia is characterized by high levels of cholesterol in the blood and is associated with an increased risk of atherosclerosis and coronary heart disease. Early detection of hypercholesterolemia is necessary to prevent onset and progress of cardiovascular disease.

Optical imaging techniques might have a potential for early diagnosis and monitoring of hypercholesterolemia. In this study, hyperspectral imaging was investigated for this application. The main aim of the study was to identify spectral and spatial characteristics that can aid identification of hypercholesterolemia in facial skin.

The first part of the study involved a numerical simulation of human skin affected by hypercholesterolemia. A literature survey was performed to identify characteristic morphological and physiological parameters. Realistic models were prepared and Monte Carlo simulations were performed to obtain hyperspectral images. Based on the simulations optimal wavelength regions for differentiation between normal and cholesterol rich skin were identified. Minimum Noise Fraction transformation (MNF) was used for analysis.

In the second part of the study, the simulations were verified by a clinical study involving volunteers with elevated and normal levels of cholesterol. The faces of the volunteers were scanned by a hyperspectral camera covering the spectral range between 400 nm and 720 nm, and characteristic spectral features of the affected skin were identified. Processing of the images was done after conversion to reflectance and masking of the images. The identified features were compared to the known cholesterol levels of the subjects.

The results of this study demonstrate that hyperspectral imaging of facial skin can be a promising, rapid modality for detection of hypercholesterolemia.

Keywords: Monte Carlo, hyperspectral imaging, hypercholesterolemia, light-tissue interaction, Minimum Noise Fraction transformation

1. INTRODUCTION

Hypercholesterolemia is characterized by high levels of cholesterol in the blood and is associated with an increased risk of atherosclerosis and coronary heart disease. Cardiovascular diseases are the leading cause of death worldwide. In 2008, 30% of all global death is attributed to cardiovascular diseases.[1] Early detection of hypercholesterolemia is necessary to prevent onset and progress of cardiovascular disease.

Hypercholesterolemia is currently diagnosed by measuring cholesterol levels in blood. For this procedure, patient must have a blood sample taken by a medical professional and interpreted by a doctor. A visit to a health care intuition can be both time consuming and expensive. Therefore it would be very convenient to have a user-friendly and easy accessible option to detect hypercholesterolemia at locations, where people usually spend some time daily, e.g. pharmacy, fitness-studio and library. A good candidate for a diagnostic modality could be an optical technique used for detecting hypercholesterolemia by measuring skin properties. The advantage of optical techniques is that they can be non-contact and non-invasive. Currently, visible and infrared spectroscopy is not used for detecting the cholesterol levels *in vivo.* The reason is the very low absorption of cholesterol in those spectral ranges, and low concentration of cholesterol in skin. A possible solution can be detection of micro-xanthelasma in facial skin. Xanthelasma is a subcutaneous soft and yellow lesion appearing in the skin around the eyes, known to be related to increased cholesterol blood levels.[2] Since the optical properties of a xanthelasma lesion differ from the properties of normal skin, reflectance information can be used for characterization. Hyperspectral imaging (HSI) might be a suitable tool for such characterization. HSI provides both spectral and spatial information in one measurement, and does not require contact between the object and the sensor. It is a promising technique in the field of medical imaging[3, 4] since it provides differentiation of tissues based on their spectral characteristics with respect to optical absorption and scattering.

The present study was carried out in a project (SEMEOTICONS, EC 7th Framework Programme, grant N° 611516) that aims to develop a novel imaging modality based on hyper- and multispectral imaging for detection of cholesterol levels in human facial skin. The goal of the study is to identify spectral and spatial characteristics that can aid identification of hypercholesterolemia in facial skin. We hypothesized that characterization of small xanthelasma, which could not be detected by visual inspection, can provide a valuable link to blood cholesterol levels. A 3D numerical model of light transport in a human skin including a xanthelasma cylinder of varying radius and thickness below the epidermis was developed. Since in a numerical study geometry and physiological state of a skin are known, simulation results provide a mean of linking the spectral features to the actual state of the skin. We computed diffuse reflectance spectrum images (DRS) for different lesion sizes and skin types. Images were obtained for multiple wavelengths in the spectral range between 400 nm and 1090 nm with wavelength step of 10 nm. The simulation results were used to develop and test a xanthelasma detection algorithm. In addition, the simulation results were evaluated *in vivo* at 11 subjects with different cholesterol levels.

2. BACKGROUND

Xanthelasma palpebrarum (Fig.1) occurs classically among middle-aged and older adults. These growths are frequently bilateral and occur frequently on the medial portions of the eyelids. They are a chronic dermatologic condition that affects less than one percent of the population.[5] In recent studies it was shown that xantelasma correlates with increased risk of cardiovascular diseases.[2, 6, 7] The evidence highlights the importance of a comprehensive physical examination and suggests that xanthelasma could be used by general clinicians to help identifying people at higher risk of cardiovascular disease.

Xanthelasma is composed of lipid-laden histiocytes that have taken up cholesterol, phospholipids and triglycerides to become foam cells. In one study they reported the following xanthelasma composition: 10% free cholesterol, 57-60% of cholesterol esters, 14-16% of phospholipids, 14% of triglycerids and 2-3% of free fatty acids.[8] Similar results were reported by other authors. The lipid-laden histiocytes are located superficially in the dermis. In a recent study information on xanthelasma thickness was presented.[9] The thickness of the xanthelasma ranged between 503 µm and 4430 µm (M = 1444 µm, SD = 716 µm).

Figure 1: A RGB image of a volunteer with xanthelasma. (Source: Wikipedia[10])

3. METHODS

3.1. Simulation of xanthelasma

The skin model was composed of four layers: a top 0.1 mm thick epidermis, a 0.1 mm thick papillary dermis, a 1.4 mm thick reticular dermis, and a semi-infinite layer of subcutaneous tissue. A xanthelasma was represented as a cylindrical insertion just beneath the epidermal layer located in the center of the volume of interest (VOI). Four different geometries of the lesions were simulated: (a) radius r = 0.50 and thickness d = 0.50 mm, (b) r = 0.50 mm and d = 0.25 mm, (c) r = 0.10 mm and d = 0.10 mm, and (e) r = 0.06 mm and d = 0.06 mm. Figure 2 presents the horizontal and vertical cross-sections of the simulated geometries.

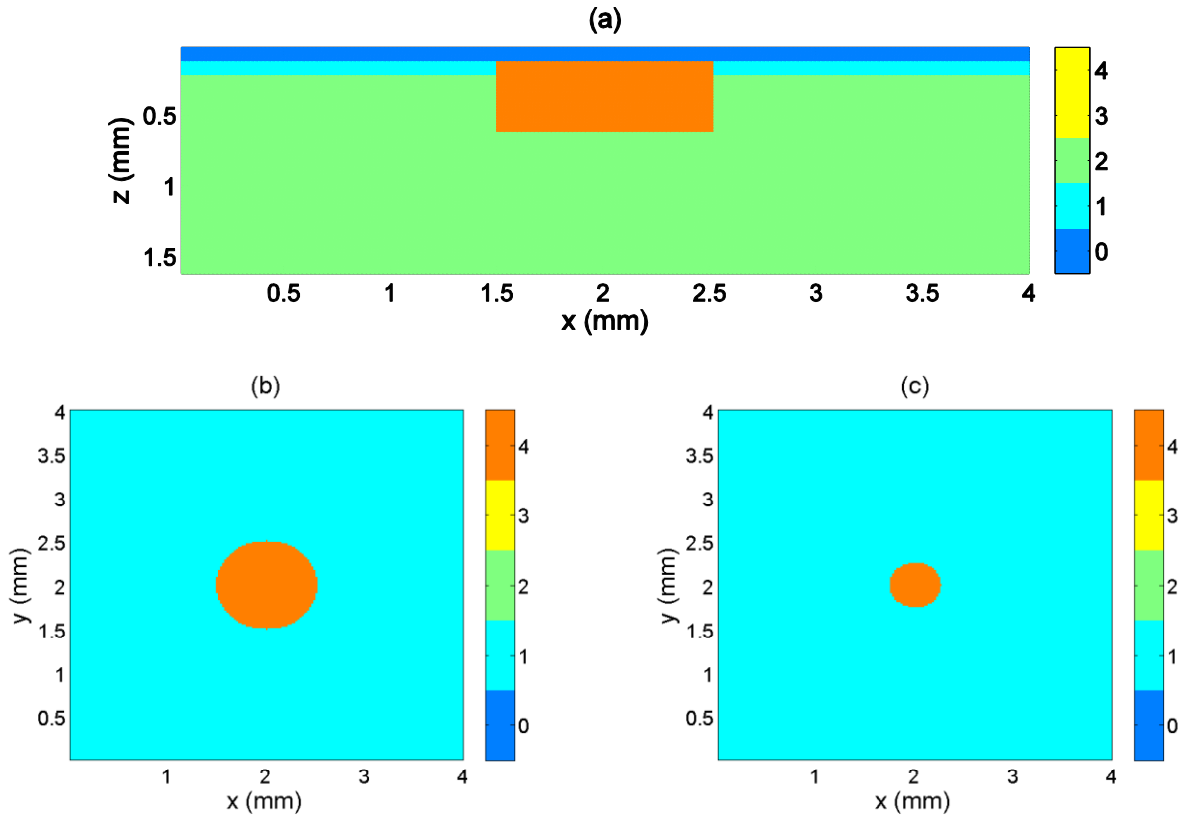

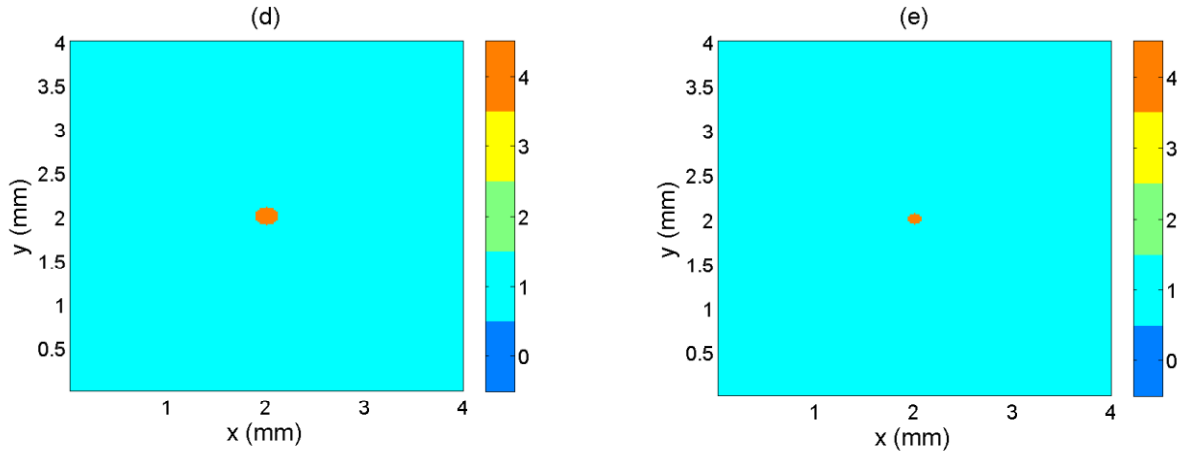

Figure 2: (a) Cross-section *xz*-plane through geometry of a skin with the largest lesion (r = 0.50 mm) through the centrum of VOI. Cross-section *xy*-planes at depth 0.1 mm of (b) r = 0.50 mm, (c) r = 0.25 mm, (d) r = 0.10 mm, and (e) r = 0.06 mm lesions. Colors represent different tissue types: (0) epidermis, (1) papillary dermis, (2) reticular dermis, (3) subcutaneous tissue, (4) xanthelasma

VOI has dimensions of 4 × 4 × 1.6 mm^3 (coordinates x, y, and z). The spatial discretization was in 0.02 mm for the all three directions, resulting in a 3D grid with 201 × 201 × 81 voxels. The geometry involve five different tissue types: (0) epidermis, (1) papillary dermis, (2) reticular dermis, (3) subcutaneous tissue, (4) xanthelasma.

For each tissue type the optical properties (μ_a, μ_s, g, and n) were found in literature.[11-14] Three melanin volume fractions (*mvf*) in the epidermal layer were simulated: 1.0%, 2.5% and 5% corresponding to a light Caucasian skin, Mediterranean skin and dark skin, respectively. The absorption coefficient of dermis depends strongly on blood volume fraction (*bvf*), oxygenation of blood (*SO2*) and water content (*wvf*) in the dermis. In the papillary dermis we used *bvf* of 0.5%, *SO2* of 50% and *wvf* of 75%. In the reticular dermis we used *bvf* of 0.5%, *SO2* of 95% and *wvf* of 75%. We simulated adipose tissue using a combination of absorption coefficients reported by van Veen et al[15] (fat) and Salomatina et al[12] (background). The chosen combination was 0.45 of fat spectrum and 0.55 of background spectrum, which resulted in diffuse reflectance spectrum presenting features present in previously measured skin spectra. Scattering coefficients were calculated using expression from Salomatina et al.[12] For anisotropy factor we used 0.78 and for index of refraction 1.44.

We approximated the optical properties of the xanthelasma by optical properties of adipose tissue.[15] This approximation is based on the composition of the xanthelasma, which is composed of cholesterol, cholesterol esters and fatty acids, all of them lipids. In addition, absorption spectrum of the pure cholesterol was measured by our group and it resembles well the spectrum of subcutaneous fat.

The simulation of the light transport in skin tissue is based on the commonly used weighted-photon Monte Carlo (MC) technique.[16] We used a custom developed 3D MC model for simulating photon transport in small volumes of skin.[17, 18] A homogenous irradiation of the skin surface was used which agrees well with the illumination conditions used in the experiment. The result of the simulation is diffuse reflectance spectrum at each point of the skin surface. The total number of simulated photons per wavelength and geometry was 30,000,000, providing acceptably low statistical noise. The number of detected photons per surface pixel depends on wavelength, but it was on average between 150 in the blue region to 500 in the 700–800 nm region. To improve the statistics, all exiting photons independent of their directions were recorded. Diffuse reflectance spectra were calculated for wavelengths between 400 nm and 1090 nm with step size of 10 nm.

3.2. Minimum Noise Fraction algorithm

The Maximum Noise Fraction transform[19] (MNF) is an algorithm commonly used for noise removal in remote sensing. It is a dimensionality reduction technique, where the data is noise whitened, and decomposed into orthogonal principal components sorted according to variance.

This can be used either to find spectral components with the highest SNR or to remove noisy components while retaining both spectral and spatial resolution. The hyperspectral image and noise band covariance statistics are used to obtain spectral components with varying levels of noise, which are subsequently used for decomposition. Results of the decompositions are MNF-eigenvectors, namely the vectors describing the transformation of a hyperspectral image and corresponding MNF-images, namely the images of the spectral components with different SNR levels.

The MNF algorithm was implemented in MATLAB 2014a (The MathWorks Inc., Natick, Massachusetts, USA).

3.3. Human subjects experiment

In the experimental part of the study, we recorded HSI of facial skin. In total, 11 volunteers with Caucasian skin type were involved in the study, 8 males and 3 females. Their age was between 25 and 61 with mean age of 46. Blood cholesterol levels of the volunteers were between 125–285 mg/dl with mean value 217 mg/dl, including all three cholesterol level classes: normal, borderline and high blood cholesterol levels. Room temperature was controlled and ranged 24-26.5 °C.

The imaging was performed by a liquid crystal tunable filter system (VariSpec™ by Cambridge Research & Instrumentation, Inc.). The spectral range was 400 – 720 nm at a step size 10 nm. The light source was a white–LED light source (R130 by Smart Vision Lights, Inc.). Images were taken from a close distance, resulting in an image containing only eyes and skin around eyes.

Image preprocessing involved three steps. An images was calibrated from raw data to reflectance using a white reflectance standard data (Spectralon® target by Labsphere, Inc.). Subsequently, a masking was applied to the image. The purpose of the masking was to eliminate parts of the image not containing skin. The Spectral Angle Mapper[20] (SAM) algorithm was used for masking. A manually selected skin spectrum was used as an endmember spectrum and a threshold of 0.99 was selected. The parts of the image not classified as a skin were filled with zeros. The final step was removing parts of the image containing exceeding specular reflection, since the specular reflection could significantly affect the analysis. The preprocessing was performed in MATLAB 2014a (The MathWorks Inc., Natick, Massachusetts, USA).

The study was approved by the National Commission for Research Ethics and Bioethics of Italy.

4. RESULTS

4.1. Simulation results

Figure 3 presents simulated spectra for all four lesions and melanin volume concentrations (*mvf*). The intact skin spectrum (*dashed black line*) is added for comparison. As expected, by increasing the lesion size the lesion spectrum becomes more different in comparison to the skin. The general trend is, that the lesion spectrum has higher reflectance due to higher scattering coefficient and lower absorption. The spectral region, where the difference is the largest is between 530 nm and 590 nm (on average 50% higher) and between 920 nm and 1080 nm (on average 20% higher). For the smallest lesion (0.12 mm), there is no evident difference between the spectra lesion and skin spectra.

The melanin concentration affects the slope of the spectra. Higher melanin concentrations result in steeper slopes. The largest effect on backscattered intensity can be observed at the shorter wavelengths, while the effects is reduced at longer wavelengths. The observed trend is due to the absorption properties of melanin. Varying melanin concentrations can significantly affect the analysis results due to a crosstalk between the required tissue parameter and the melanin. Therefore

information about *mvf* can be of importance for interpretation and correction of the results. The observable noise in the simulated spectra is the consequence of stochastic nature of the MC simulation.

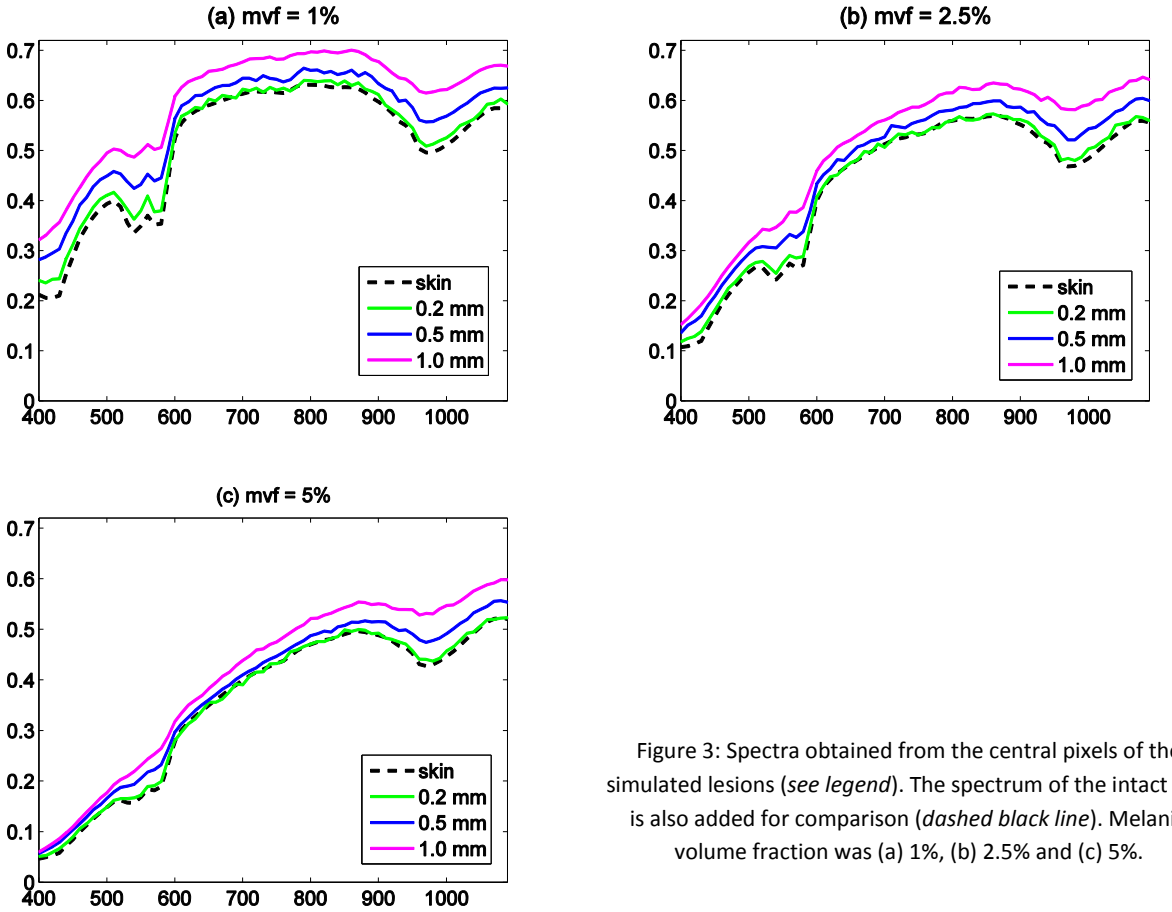

Figure 3: Spectra obtained from the central pixels of the simulated lesions (*see legend*). The spectrum of the intact skin is also added for comparison (*dashed black line*). Melanin volume fraction was (a) 1%, (b) 2.5% and (c) 5%.

For each size of the lesions, we combined three images obtained at different *mvf* into one hyperspectral image. The order of the sub-images was: bottom, middle and top for 1%, 2.5% and 5% *mvf*, respectively. The reason for combining different *mvf* sub-images in the same image was to separate the *mvf* spectral features from other spectral features. The combined images served as inputs in the MNF algorithm. The output of the algorithm were MNF-eigenvectors representing different spectral features, and the corresponding MNF-images. The latter are the hyperspectral images projected on the MNF-eigenvector space.

Figure 4 presents the MNF-images and the corresponding MNF-eigenvectors for the 0.5 mm lesion. Similar results were obtained for other lesions, except the 0.12 mm lesion. For the latter, the lesion was not enhanced in any of the MNF-images. Evidently, the first MNF-image (Fig.4a) corresponds to *mvf*, while the third MNF-image enhances the lesions. The 2nd and 4th MNF-image show a combination of *mvf* and lesions. The corresponding MNF-eigenvectors are presented below the MNF-images. The components number 5 and higher do not contain any valuable information but noise.

In the 3rd MNF-component, lesions are much brighter than the skin, which is uniformly black. The brightness of the lesions is not equal for all the lesions even though the lesions have the same geometry and composition. It tends to get less bright with increasing *mvf*. This trend is due to the crosstalk between melanin in the epidermis and fat in the lesion.

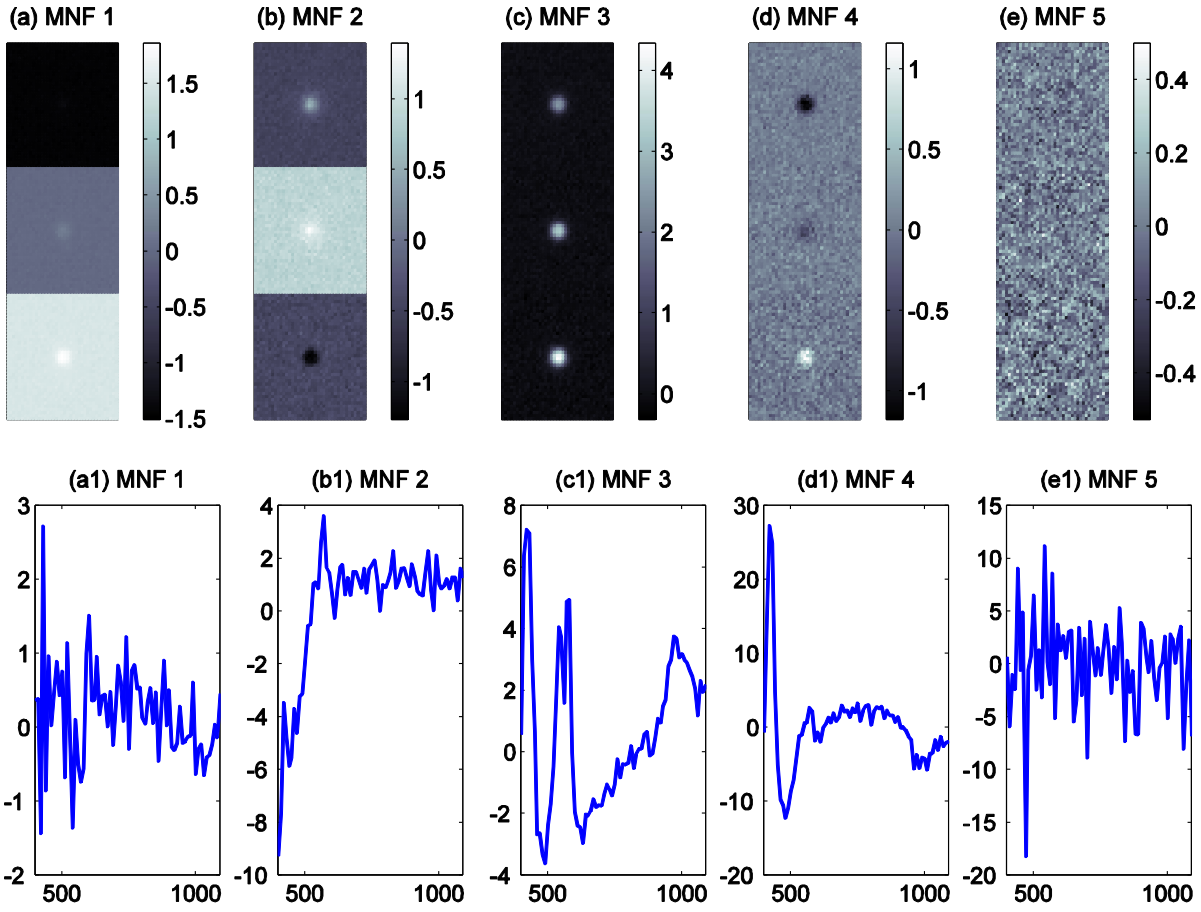

Figure 4: (a–e) MNF-images 1–5 of the simulated 0.5 mm xanthelasma. (a1-e1) Corresponding MNF-eigenvectors. Melanin concentrations: 1% (bottom), 2.5%(middle), 5% (top).

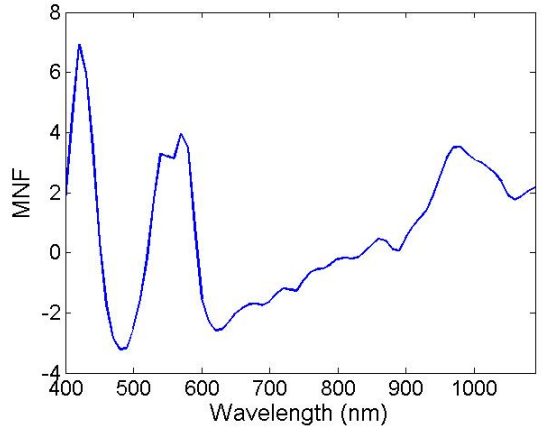

Figure 5: A smoothed xanthelasma MNF-eigenvector for the full spectral range.

The same MNF-eigenvector enhancing xanthelasma was obtained independent of the lesion size. We smoothed the xanthelasma eigenvector (Fig.5) using a smoothing function *smooth* available in MATLAB (version 2014a,

MathworksTM, MA). The *lowess* filter with 20 point was used. The eigenvector features positive and negative components between 420 nm and 480 nm, positive components between 540 nm – 590 nm (compensating hemoglobin peaks), increasing slope from 600 nm on (compensating melanin absorption) and a peak at 970 nm (compensating water).

The smoothed xanthelasma eigenvector was used to project out the lesions in the simulated hyperspectral data. The projection is essentially a pixel-wise multiplication of an image with the eigenvector. Evidently, all lesions are clearly projected out (Fig.6). Moreover, the smallest lesion can be also distinguished. Yet, the background in case of the 0.12 mm lesion is almost at the level of the lesion and contains a lot of noise, thus applying a proper threshold can be problematic.

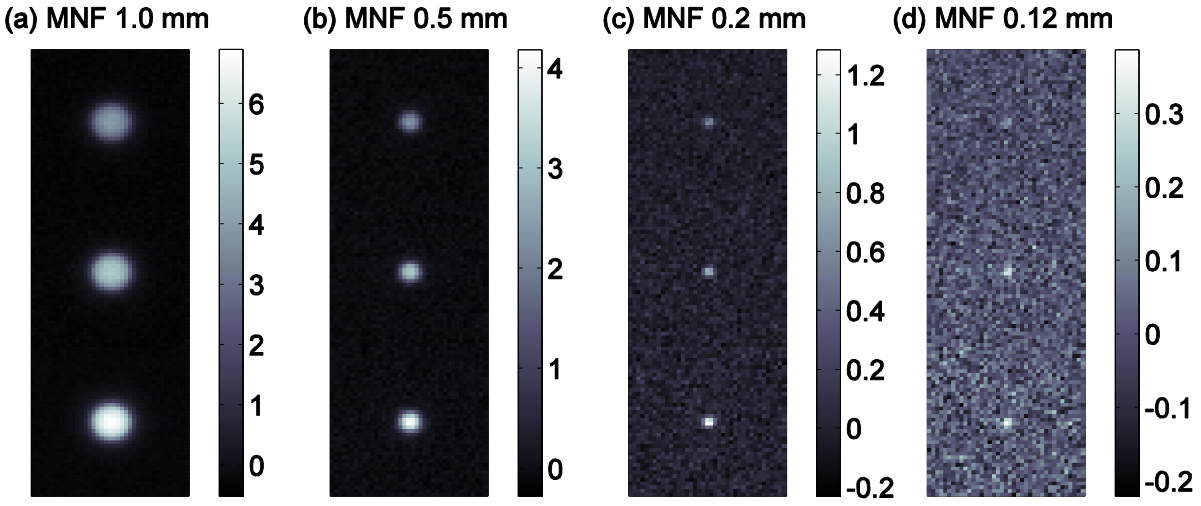

Figure 6: (a–d) HSI of 1.0 mm to 0.12 mm lesions projected on the smoothed xanthelasma eigenvector. Melanin concentrations: 1% (bottom), 2.5%(middle), 5% (top).

4.2. Experimental results

The MNF algorithm was also tested on experimental data. Similar to the simulation data analysis, we constructed a large image containing hyperspectral sub-images from all 11 volunteers. Sub-images were 500×200 pixel images of the skin under left eyes. For the presentation purpose, we also constructed an image presenting the volunteer information at the same locations as the skin sub-images were (Fig.7a). Here the following information is presented: *V* – volunteer number, *M/F* – male or female, *number* – age, *Chol* – total blood cholesterol in (mg/dl), *LDL* – blood low density lipoprotein concentration in (mg/dl), *HDL* – blood high density lipoprotein concentration in (mg/dl), *TAG* – blood lipids concentration in (mg/dl), *bil* – total bilirubin concentration (mg/dl). The color coding is: *blue* – normal cholesterol level (up to 200 mg/dl), *cyan* – borderline cholesterol level (200–240 mg/dl) and *yellow* – hypercholesterolemia (more than 240 g/dl). The color coding for the text is: *black* – normal concentration, *green* – slightly elevated, *magenta* – borderline, *red* – excess value.

Figure 7b presents the corresponding RGB image constructed from the HSI data. The dark patches in the image are due to the removal of the specular reflectance. Evidently, a visual inspection of the RGB image cannot provide a mean to determine the increased levels of cholesterol.

The spectral range used for the MNF algorithm testing was 450–720 nm. A visual inspection of the MNF-images shows that the 3rd MNF-image correlates with the cholesterol levels (Fig.7c). Here, the sub-images of the volunteers 14,19 and 23, which has hypercholesterolemia, are brighter than other images.

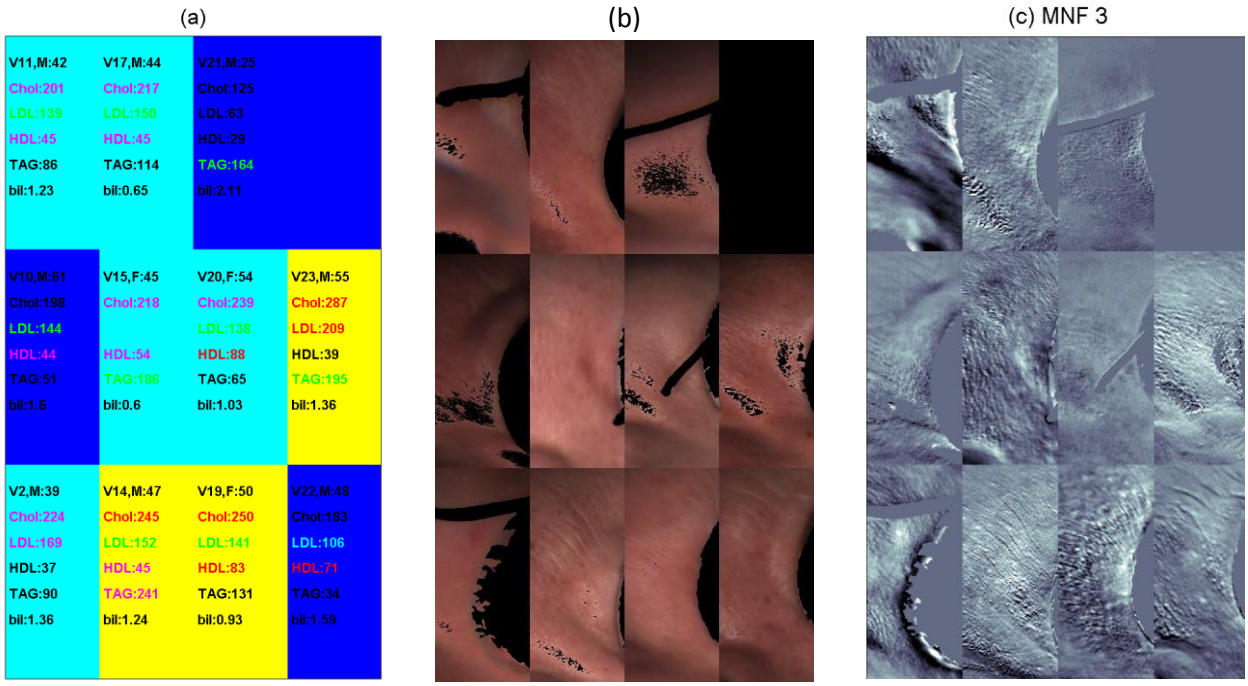

Figure 7: (a) Image presenting the volunteers information (see text for explanation), (b) corresponding RGB image, (c) 3rd MNF transformation image. The color coding for cholesterol is: *blue* – normal cholesterol level (up to 200 mg/dl), *cyan* – borderline cholesterol level (200–240 mg/dl) and *yellow* – hypercholesterolemia (more than 240 g/dl).

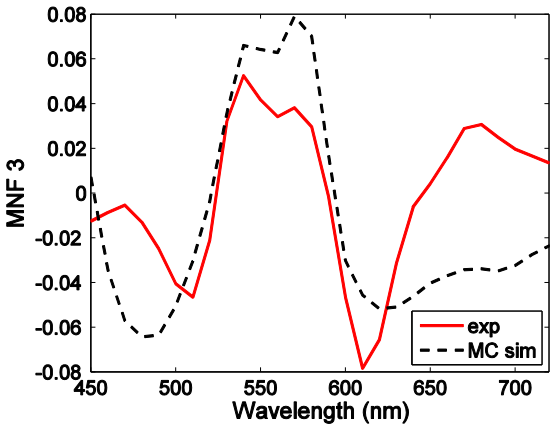

Figure 8: 3rd MNF-eigenvector obtained from the experimental data. The corresponding MNF-eigenvector for the simulated data is presented for comparison.

Figure 8 presents the 3rd MNF-eigenvector from the experimental data (*red line*) and the corresponding simulation MNF-eigenvector (*black dashed line*). Both MNF-eigenvectors have similar features, especially in the region 510 – 610 nm. The differences between the two eigenvectors might be due to the differences between experimental conditions (camera properties, light source properties) and the simulated conditions. Additional reason for these differences can also be inadequate calibration of the experimental data.

We normalized the 3rd MNF-image (Fig.7c), so the values were within the 0 – 1.0 range. Next, we applied 0.2 threshold to the normalized image. The result was a black-white image showing only pixels with values larger than the threshold (Fig.9).

Figure 9: The xanthelasma enhanced image with a threshold of 0.2 applied.

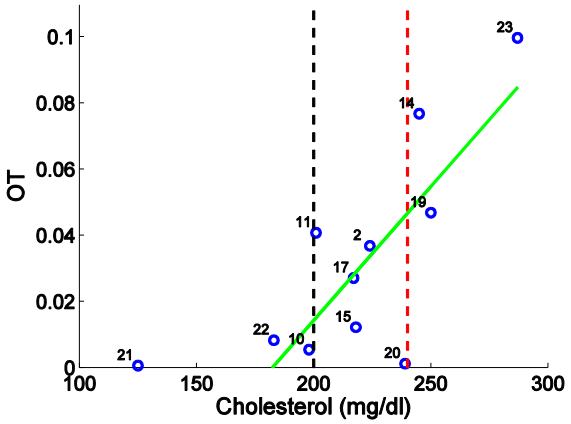

Figure 10: Measured blood cholesterol levels compared to OT values determined from the MNF analysis. The black dashed line represents normal cholesterol limit (200 mg/dl) and the red dashed line represents the borderline cholesterol level blood concentration (240 mg/dl). The green line represents linear fit of the data. The volunteer numbers are written besides the circles.

For each sub-image we calculated a fraction of the pixels over threshold and named it *OT* (Fig.10). The dependency is almost linear, except the values for volunteers 11 and 20. The linear fit expression is $OT = (8.1 \pm 2.5) \cdot 10^{-4} \cdot CL - 0.1476 \pm 0.0563$, where *CL* represents cholesterol level. The p-value of the fit is 0.0112 indicating strong presumption against the null hypothesis. The R-squared is 0.573, also indicating a reasonably good fit. The reason that the volunteer 11 had a high OT value can be the inadequate masking, resulting in some of the eye protection googles image being included in the analysis (see Fig.7b). The reason why the volunteer 20 had a very low value is not known. However, according to the clinical studies[2, 7], the correlation between xanthelasma and elevated cholesterol blood level is not absolute, therefore some deviations from the expected trend are normal.

The MNF algorithm showed a surprisingly good performance at detection of lipid deposits both in the simulated and experimental data. The difference between datasets is the spectral range. For the simulated data it was 400–1090 nm, while for the experimental it was 450–720 nm. Therefore we repeated the analysis of the simulated data using a reduced, 450–720 nm, spectral range. The outcome of the analysis was the same as for the full spectral range. The only difference is that the reduced spectral band approach results have higher noise.

While analyzing the simulated data we found that the brightness of the lesions in the MNF-images depend on *mvf*. Since comparable levels of brightness are desired for the same concentration of lipids, the brightness level should be adjusted based on the *mnf* level. *mnf* levels can be determined using the 1st MNF-eigenvectors or other algorithms (e.g., inverse diffusion approximation)[21]. Thus finding an appropriate adjustment procedure would be one of our future tasks.

The experimental dataset presented here included only skin under the left eyes of the volunteers. The next step is to analyze all available skin to validate the method. In addition, more advanced statistical tools will be used to confirm the correlation between the actual cholesterol blood levels and the determined OT values.

5. CONCLUSIONS

In this study we present performance of hyperspectral imaging at detection of elevated cholesterol blood levels. We focused on lipid deposits which are typically found below the epidermis in the skin around the eyes, micro-xanthelasmas. We simulated hyperspectral images of xanthelasma and tested the MNF-algorithm using the simulated data. Analyzing the MNF algorithm results we identified a suitable transformation of the images which enhanced the lipid deposits. The transformation very efficiently eliminated the effect of melanin and other chromophores visualizing only the lesions. We verified the approach using an experimental dataset, including hyperspectral images of volunteers with different cholesterol blood levels. Similar results were obtained for the experimental data. To quantify the experimental results, we determined an index calculated from the xanthelasma enhanced images and correlated it to the actual cholesterol blood levels. A good agreement was found. The results of this study demonstrate that hyperspectral imaging can be a promising, rapid modality for detection of hypercholesterolemia.

ACKNOWLEDGEMENTS

This work was supported by the European Commission under the 7th Framework Programme for the Collaborative project under grant agreement N° 611516 (SEMEOTICONS).

The authors would thank Giuseppe Coppini and the rest of the team from CNR-ISTI and CNR-IFC for making the experimental part possible.

REFERNCES

[1] Organization, W. H., [Cardiovascular diseases (CVDs)], (2013) http://www.who.int/mediacentre/factsheets/fs317/en/.

[2] Fernandez, A. B.,Thompson, P. D., "Eye markers of cardiovascular disease," British Medical Journal, 343, (2011).

[3] Sorg, B. S., Moeller, B. J., Donovan, O., Cao, Y.,Dewhirst, M. W., "Hyperspectral imaging of hemoglobin saturation in tumor microvasculature and tumor hypoxia development," J Biomed Opt, 10(4), 44004 (2005).

[4] Randeberg, L. L., Larsen, E. L. P.,Svaasand, L. O., "Hyperspectral imaging of blood perfusion and chromophore distribution in skin," Photonic Therapeutics and Diagnostics V, 7161, (2009).

[5] Durairaj, V. D.,Hall, J. A., "Multiple yellow plaques of the eyelids," American Journal of Medicine, 119(1), 34-35 (2006).

[6] Noel, B., "Premature atherosclerosis in patients with xanthelasma," Journal of the European Academy of Dermatology and Venereology, 21(9), 1244-1248 (2007).

[7] Christoffersen, M., Frikke-Schmidt, R., Schnohr, P., Jensen, G. B., Nordestgaard, B. G.,Tybjaerg-Hansen, A., "Xanthelasmata, arcus corneae, and ischaemic vascular disease and death in general population: prospective cohort study," British Medical Journal, 343, (2011).

[8] Vermeer, B. J., Mateysen, A. A. E., Vangent, C. M., Vansabben, R. M.,Emeis, J. J., "The Lipid-Composition and Localization of Free and Esterified Cholesterol in Different Types of Xanthomas," Journal of Investigative Dermatology, 78(4), 305-308 (1982).

[9] Mittelviefhaus, H., Kreusser, C., Bohringer, D.,Auw-Hadrich, C., "The Underestimated Depth of Tissue Invasion of Xanthelasma - a Histological Study," Klinische Monatsblatter Fur Augenheilkunde, 228(1), 14-18 (2011).

[10] Wikimedia, [Xanthelasma], (2015) https://en.wikipedia.org/wiki/Xanthelasma.

[11] Jacques, S. L., "Optical properties of biological tissues: a review," Physics in Medicine and Biology, 58(11), R37-R61 (2013).

[12] Salomatina, E., Jiang, B., Novak, J.,Yaroslavsky, A. N., "Optical properties of normal and cancerous human skin in the visible and near-infrared spectral range," J Biomed Opt, 11(6), (2006).

[13] Patwardhan, S. V., Dhawan, A. P.,Relue, P. A., "Monte Carlo simulation of light-tissue interaction: Three-dimensional simulation for trans-illumination-based Imaging of skin lesions," Ieee Transactions on Biomedical Engineering, 52(7), 1227-1236 (2005).
[14] Ding, H. F., Lu, J. Q., Wooden, W. A., Kragel, P. J.,Hu, X. H., "Refractive indices of human skin tissues at eight wavelengths and estimated dispersion relations between 300 and 1600 nm," Physics in Medicine and Biology, 51(6), 1479-1489 (2006).
[15] van Veen, R. L. P., Sterenborg, H. J. C. M., Pifferi, A., Torricelli, A.,Cubeddu, R., [Determination of VIS- NIR absorption coefficients of mammalian fat, with time-and spatially resolved diffuse reflectance and transmission spectroscopy], (2004).
[16] Wang, L., Jacques, S. L.,Zheng, L., "MCML--Monte Carlo modeling of light transport in multi-layered tissues," Comput Methods Programs Biomed, 47(2), 131-46 (1995).
[17] Milanic, M.,Majaron, B., "Three-dimensional Monte Carlo model of pulsed-laser treatment of cutaneous vascular lesions," J Biomed Opt, 16(12), (2011).
[18] Bjorgan, A., Milanic, M.,Randeberg, L. L., "Estimation of skin optical parameters for real-time hyperspectral imaging applications," Journal of Biomedical Optics, submitted (2014).
[19] Green, A. A., Berman, M., Switzer, P.,Craig, M. D., "A Transformation for Ordering Multispectral Data in Terms of Image Quality with Implications for Noise Removal," Ieee Transactions on Geoscience and Remote Sensing, 26(1), 65-74 (1988).
[20] Kruse, F. A., Lefkoff, A. B., Boardman, J. W., Heidebrecht, K. B., Shapiro, A. T., Barloon, P. J.,Goetz, A. F. H., "The Spectral Image-Processing System (Sips) - Interactive Visualization and Analysis of Imaging Spectrometer Data," Remote Sensing of Environment, 44(2-3), 145-163 (1993).
[21] Svaasand, L. O., Norvang, L. T., Fiskerstrand, E. J., Stopps, E. K. S., Berns, M. W.,Nelson, J. S., "Tissue Parameters Determining the Visual Appearance of Normal Skin and Port-Wine Stains," Lasers in Medical Science, 10(1), 55-65 (1995).